Mesoporous Cathodes

DOI: 10.1002/ange.200803431

# Synthesis of Ordered Mesoporous Li–Mn–O Spinel as a Positive Electrode for Rechargeable Lithium Batteries**

*Feng Jiao, Jianli Bao, Adrian H. Hill, and Peter G. Bruce**

$LiMn_2O_4$ spinel is one of the most important intercalation electrodes for rechargeable lithium batteries at the present time.[1–4] It combines the highest intrinsic rate capability of the well-known intercalation cathodes with high safety, low toxicity, and low cost, making it attractive for high-power applications, such as hybrid electric vehicles.[5–11] However, the drawback of this electrode is its slow dissolution in the electrolyte present in the lithium-ion battery. To mitigate such dissolution, recent interest has focused on highly lithium-rich compositions in the region of $Li_{1.12}Mn_{1.88}O_4$ ($Li[Li_{0.12}Mn_{1.88}]O_4$) because of their high average oxidation state (presence of less soluble $Mn^{3+}$), despite compromising theoretical capacity.[11,12] Consequently, high rate capability becomes even more important to ensure high utilization of the reduced theoretical capacity. Here we describe the synthesis of an ordered mesoporous $Li_{1.12}Mn_{1.88}O_4$ spinel and show that it combines higher rate capability than the corresponding bulk material (50% higher specific capacity at a rate of 30C, 3000 mA $g^{-1}$) at ambient temperature with good stability at elevated temperatures, despite a high surface area of 90 $m^2 g^{-1}$ and without the need for deliberate coating or doping with foreign ions.[13,14] Furthermore, when cycled over a wide voltage range (including the 3 V and 4 V plateaus) the mesoporous material exhibits improved capacity retention compared to the bulk spinel. This capacity retention is because of the nanometer thin walls between the pores that render the cubic/tetragonal phase transformation more facile in the mesoporous spinel than in the bulk phase. The potential advantages of using nanostuctured electrode materials, in this case mesoporous solids, over nanoparticles are discussed.

Ordered mesoporous $Li_{1+x}Mn_{2-x}O_4$ spinel is synthesized for the first time, as described in detail in the Experimental Section, by a hard templating route with post-template treatment.[15–19] Briefly, an aqueous solution of $Mn(NO_3)_2$ was infiltrated into the ordered 3D pore structure of the mesoporous silica, KIT-6. Heating in air converted the precursor into $Mn_2O_3$. Following the removal of the $SiO_2$ template, the replica 3D mesoporous $Mn_2O_3$ was transformed to $Mn_3O_4$ spinel by heating in a reducing atmosphere, which then reacted with LiOH to form mesoporous $LiMn_2O_4$ spinel (Figure 1). It is remarkably that throughout the solid-state

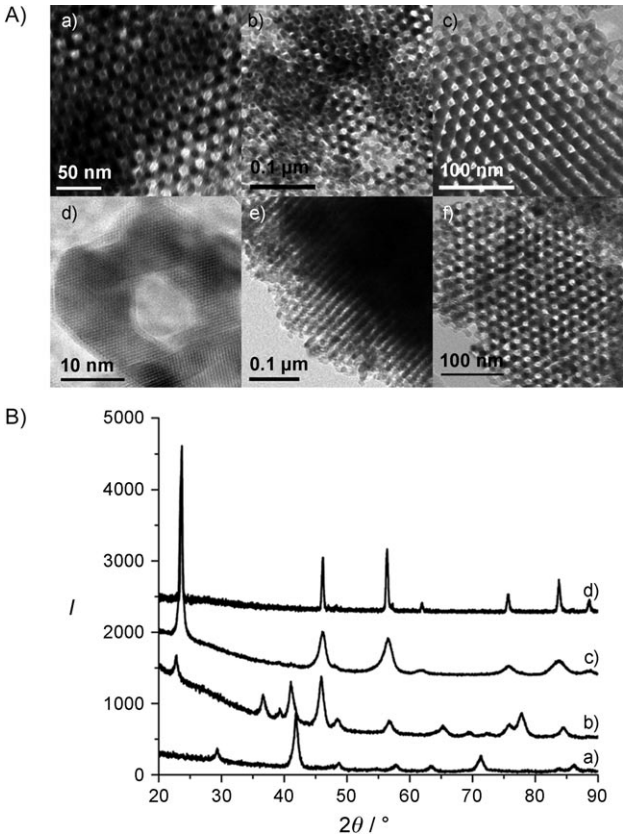


***Figure 1.*** A) TEM images of mesoporous a) $Mn_2O_3$, b) $Mn_3O_4$, and c) $Li_{1.12}Mn_{1.88}O_4$. d) High-resolution TEM image of mesoporous $Li_{1.12}Mn_{1.88}O_4$. e,f) TEM images of mesoporous $Li_{1.12}Mn_{1.88}O_4$ e) after 20 cycles between 3–4.3 V and f) after 30 cycles between 2–4.5 V. B) Powder XRD patterns of mesoporous a) $Mn_2O_3$, b) $Mn_3O_4$, c) $Li_{1.12}Mn_{1.88}O_4$, broadened owing to nanometer-thin walls, and d) bulk $Li_{1.12}Mn_{1.88}O_4$.

transformations $Mn_2O_3 \rightarrow Mn_3O_4 \rightarrow LiMn_2O_4$, the ordered 3D mesoporous structure was preserved (Figure 1), demonstrating that the thin walls of the mesopore (7 nm thick) can accommodate the strain of multiple solid–solid phase transformations. The mesoporous structure exists throughout the material, as demonstrated by examining many particles using

[*] Dr. F. Jiao,[+] J. Bao, Prof. P. G. Bruce
EaStChem and School of Chemistry, University of St. Andrews
The Purdie Building, North Haugh, St Andrews KY16 9ST (UK)
E-mail: g.bruce@st-and.ac.uk
A. H. Hill
School of Chemistry and EaStChem, University of Edinburgh,
Joseph Black Building
West Mains Road, Edinburgh EH9 3JJ (UK)
[+] Current address: Physical Biosciences Division, Lawrence Berkeley National Laboratory
1 Cyclotron Rd, Berkeley, CA 94720 (USA)

[**] P.G.B. is indebted to the EPSRC (SUPERGEN) and the EU for financial support. A.H.H. would like to thank Dr. Ronald Brown for the assistance with the XPS setup.

Supporting information for this article is available on the WWW under http://dx.doi.org/10.1002/anie.200803431.

TEM. The strategy of post-template reduction followed by solid-state reaction with LiOH permitted the synthesis of a mixed-valence lithium-containing compound that could otherwise not be easily synthesized directly within the template. Control of the oxygen partial pressure within the pores of the $SiO_2$ template to control the mixed-valance state, would have proved difficult, and introduction of a lithium precursor within the silica template would, on heating, have led to its reaction with the silica. Circumventing the latter problem has been demonstrated only once before by synthesizing the low temperature (LT) form of $LiCoO_2$.[16] However, LT-$LiCoO_2$ is a poor cathode with low capacity, and in contrast to manganese spinel, is of limited interest.[3,4]

The mesoporous spinel has the same cubic mesostructure as KIT-6 (space group *Ia3d*). An $a_0$ lattice parameter of 24.1 nm for the spinel was extracted from the TEM data. $N_2$ sorption measurements conducted on the mesoporous spinel (see Supporting Information) show a type IV isotherm, as observed in mesoporous materials. Barrett–Joyner–Halenda (BJH) analysis of the desorption isotherm indicated a pore size distribution with a peak centered at 4.1 nm. Such a pore diameter for the mesoporous spinel is in good agreement with the dimensions of the walls of the KIT-6 template, which become the pores of the replica spinel structure. The BET surface area for mesoporous $Li_{1.12}Mn_{1.88}O_4$ is 90 $m^2 g^{-1}$, which is similar to that of other mesoporous transition metal oxides templated by KIT-6.[20–25]

Chemical/oxidation state analysis (see Experimental Section) indicated that the composition of the spinel phase was $Li_{1.12}Mn_{1.88}O_4$. The powder XRD pattern shown in Figure 1 B (c), confirms the spinel structure and is in agreement with that of the bulk $Li_{1.12}Mn_{1.88}O_4$, although the mesoporous material exhibits peak broadening as expected for a nanomaterial.[26] Although using the highest temperature commensurate with retention of the mesostructure (400 °C), and strong reducing conditions ($H_2$ gas), it was not possible to synthesize a more reduced spinel with a composition closer to stoichiometric $LiMn_2O_4$.

Lithium manganese oxide spinel may be cycled over 3 V and 4 V plateaus.[1,2,27] Cycling in the more technologically relevant 4 V region will be considered first, and thereafter the effect of the mesostructure on cycling over both plateaus.

Mesoporous $Li_{1.12}Mn_{1.88}O_4$ was incorporated into a composite electrode as described in the Experimental Section. Additional electrodes were constructed identically (same composition and active mass), except for replacement of the mesoporous spinel with bulk spinel of the same composition. Another bulk spinel, $Li_{1.05}Mn_{1.95}O_4$, with a composition regarded as within the range for optimum performance has also been used.[8–10] Both bulk materials were prepared by a solid-state reaction (Experimental Section). To compare directly the rate capabilities of the three different spinel materials, their discharge capacities on the first cycle were expressed as a percentage of their capacity at a rate of 30 mA $g^{-1}$ (0.30C; 1C equates to discharge of the theoretical capacity of $Li_{1.12}Mn_{1.88}O_2$, 98 mA $g^{-1}$, in 1 h) and plotted versus current density in Figure 2 A. Use of the same loading of active material per unit area in each case resulted in a thicker mesoporous electrode because of the lower density of the porous material. As can be seen from the Figure 2 A, the mesoporous material exhibits the best capacity retention at

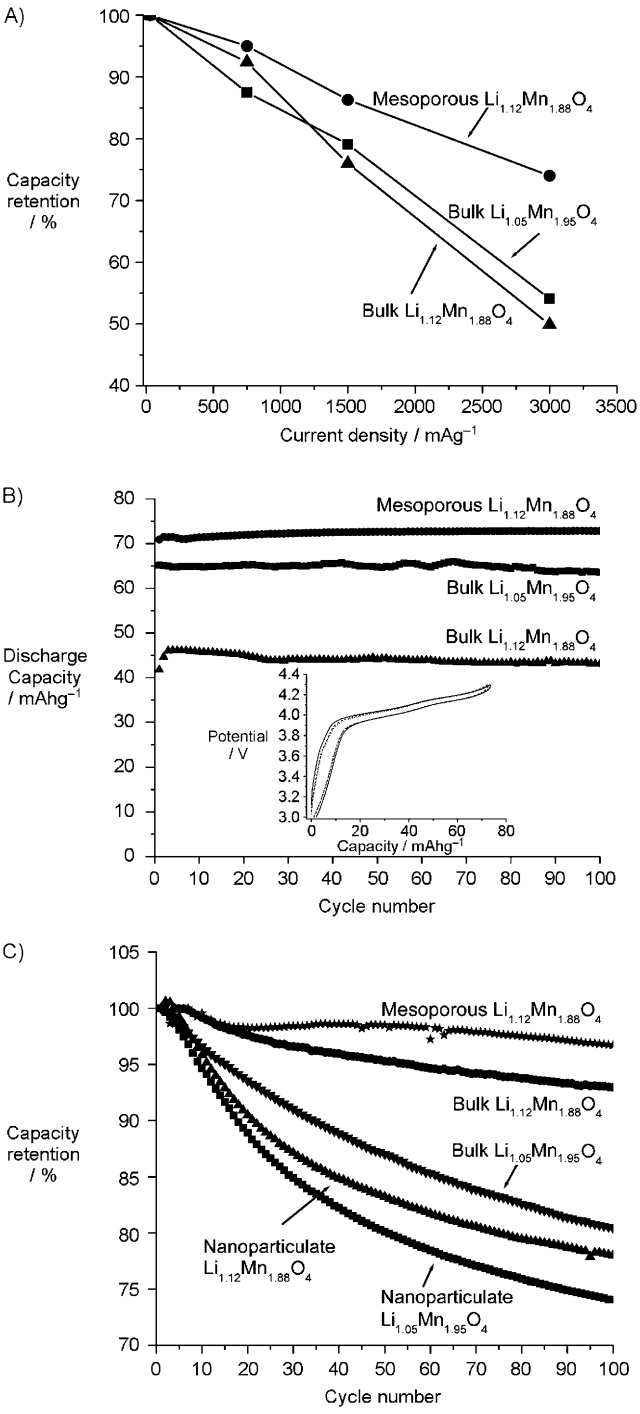


***Figure 2.*** A) Rate capability for mesoporous $Li_{1.12}Mn_{1.88}O_4$ (●), bulk $Li_{1.05}Mn_{1.95}O_4$ (■), and bulk $Li_{1.12}Mn_{1.88}O_4$ (▲); capacity retention expressed as percentage capacity at 30 mA $g^{-1}$ (0.30C). B) Cycling data for mesoporous $Li_{1.12}Mn_{1.88}O_4$ (●), bulk $Li_{1.05}Mn_{1.95}O_4$ (■), and bulk $Li_{1.12}Mn_{1.88}O_4$ (▲) between 3–4.3 V at a rate of 3000 mA $g^{-1}$ (30C). The inset shows the load curves, 5th cycle (——), 25th cycle (– – –), and 50th cycle (•••••) for mesoporous $Li_{1.12}Mn_{1.88}O_4$. C) Cycling data for mesoporous $Li_{1.12}Mn_{1.88}O_4$ (⋆), bulk $Li_{1.12}Mn_{1.88}O_4$ (●), bulk $Li_{1.05}Mn_{1.95}O_4$ (▼), nanoparticulate $Li_{1.12}Mn_{1.88}O_4$ (▲),and nanoparticulate $Li_{1.05}Mn_{1.95}O_4$ (■) at 50 °C at 30 mA $g^{-1}$ (0.30C) between 3–4.3 V.

  

high rates, despite having a thicker electrode. Its capacity retention is 50% higher than the equivalent $Li_{1.12}Mn_{1.88}O_2$ bulk phase at a rate of 3000 mA $g^{-1}$ (30C), demonstrating the superior rate capability obtained by using a mesoporous spinel. No attempt has been made to optimize the electrode construction, and thus we do not claim that these are the best performances that can be obtained for spinel electrodes.[10] Rather, all the electrodes are constructed identically to facilitate back-to-back comparison of the effect of mesoporosity on the performance, not to demonstrate the best possible performance.

The superior rate capability of the mesoporous material may be due to a number of factors. The higher surface area in contact with the electrolyte (BET surface area for mesoporous $Li_{1.12}Mn_{1.88}O_4$ is 90 $m^2 g^{-1}$ compared with 1.5 $m^2 g^{-1}$ for the bulk forms of the two compositions) and the thin walls, resulting in short diffusion lengths of approximately 3.5 nm (wall thickness 7 nm), are clearly important. However, in addition, the ordered cubic pore structure ensures that the pores are of uniform size and uniformly interconnected in all directions, thus helping to promote efficient and equal access of the electrolyte to the internal surface throughout the electrode.

The conventional approach to optimizing the power (rate) of an electrode is to reduce the particle size to a few nanometers. It is interesting to compare the rate performance of the electrodes consisting of nanoparticles with those in which the particles are mesoporous and are of micrometer dimensions, the internal walls being a few nanometers thick. Ultimately, obtaining high power (rate) in any electrode requires porosity to ensure a ready supply of ions from the electrolyte and thus sacrificing volumetric capacity is the inevitable price to pay for high rate. If this is achieved by deliberately designing porosity inside the particles, as in the mesoporous solids, then an optimum pore size may be selected such that volume of the solid will not be unnecessarily wasted, as in the case of solids with random porosity (random in size and shape). Random porosity also gives rise to situations in a composite electrode made of nanoparticles, in which some pores will be too small, too large, or occluded. As the particles of the mesoporous solid are of micron dimensions, they maintain a similar interparticle contact to that of bulk materials and will pack more densely within the composite electrode than nanoparticles. It is recognized that fabricating electrodes from nanoparticles is difficult because of the low tap density and problem of maintaining particle contact. Of course a potential disadvantage is that preparing mesoporous materials may be more difficult than simple nanoparticles. Comparison between mesoporous $Li_{1.12}Mn_{1.88}O_4$ and an electrode constructed identically with bulk $Li_{1.05}Mn_{1.95}O_4$, indicates that the rate capability of the mesoporous material is also superior to this bulk composition (Figure 2A).

Recent interest in Li–Mn–O spinel arises from its high rate capability and thus its usefulness for high-rate applications. Thus, the focus was on cycling at high rate (power). The absolute capacities for the three materials at the high rate of 3000 mA $g^{-1}$ (30C) are shown in Figure 2B, from which it may be seen that the specific capacity of the mesoporous material is significantly higher than its bulk equivalent (by 50–60%) and somewhat higher than bulk $Li_{1.05}Mn_{1.95}O_4$ despite a lower theoretical capacity for $Li_{1.12}Mn_{1.88}O_2$ because of its more lithium-rich composition. Considering the effect of the mesoporosity on the volumetric capacity, the density of mesoporous $Li_{1.12}Mn_{1.88}O_4$ is 35% lower than the corresponding bulk material, which translates into a 25% reduction in volumetric capacity of the composite electrode, as only a proportion of the composite electrode is the active material. Thus, based on the total volume of the electrode, those constructed using mesoporous $Li_{1.12}Mn_{1.88}O_4$ have a higher gravimetric and slightly higher volumetric energy density than those fabricated using the corresponding bulk material. The inset in Figure 2B shows the load curves for 3 cycles (5, 25, and 50) of the mesoporous Li-1.12 phase. The difficulty in resolving one cycle from another emphasizes the stability of the load curves on cycling. Retention of the mesostructure on cycling is demonstrated by the TEM data in Figure 1A (e).

Having considered the performance at 30 °C it is interesting to examine the performance at elevated temperatures. It is well known that $Mn^{3+}$ disproportionation into $Mn^{2+}$ and $Mn^{4+}$, followed by $Mn^{2+}$ dissolution in the electrolyte, is one of the main causes of spinel electrodes losing capacity with time/cycling in cells operated at elevated temperatures of circa. 50 °C. Lowering of the cell capacity is particularly severe if graphite electrodes are employed.[13,14,28] To alleviate such the capacity lowering, Li–Mn–O spinels may be doped with foreign ions, for example $F^-$, or coated with metal oxides, such as ZnO.[29,30] As a result, mesoporous $Li_{1.12}Mn_{1.88}O_4$, with its high surface area and without such modifications, might have been expected to exhibit severed capacity loss on cycling at elevated temperatures.

To investigate the elevated temperature stability of the mesoporous phase, the variation of discharge capacity with cycle number at 50 °C is shown in Figure 2C for 1) mesoporous, 2) nanoparticle, 3) bulk $Li_{1.12}Mn_{1.88}O_4$, 4) nanoparticle, and 5) bulk $Li_{1.05}Mn_{1.95}O_4$. The capacities are presented as a percentage of their theoretical values, to provide direct comparison of the lowering of the capacity on cycling for the different materials. A low rate of 30 mA $g^{-1}$ was selected to provide a more severe test of capacity fading on cycling than would be the case if high rates were employed. The rapid loss of capacity on cycling the bulk $Li_{1.05}Mn_{1.95}O_4$ is evident in Figure 2C and is in accord with previous studies of such optimized nonstoichiometric spinels in the absence of foreign ion dopants or coatings.[10,13,31] Nanoparticles of $Li_{1.05}Mn_{1.95}O_4$ (BET surface area of 40 $m^2 g^{-1}$ compared with 1.5 $m^2 g^{-1}$ for the bulk material) result in even more severe capacity fading (Figure 2C). Nanoparticles of $Li_{1.12}Mn_{1.88}O_4$ (40 $m^2 g^{-1}$) show lowering of the capacity to some extent and the lowering takes place presumably because of the higher average oxidation state leading to a higher $Mn^{4+}/Mn^{3+}$ ratio at the surface. Thus, the $Mn^{3+}$ disproportionation reaction is lowered leading to lesser $Mn^{2+}$ dissolution in the electrolyte. However, the mesoporous $Li_{1.12}Mn_{1.88}O_4$ material exhibits roughly comparable capacity retention to the corresponding bulk material (surface area 1.5 $m^2 g^{-1}$; Figure 2C), despite the former having a surface area twice that of the $Li_{1.12}Mn_{1.88}O_4$ nanoparticles (90 $m^2 g^{-1}$ compared with 40 $m^2 g^{-1}$). This could

  

be in part due to the micrometer-sized particles of the mesoporous material, which may maintain better interparticle contact than the nanoparticles on cycling. However, we suggest that the comparable capacity retentions of the mesoporous and the bulk $Li_{1.12}Mn_{1.88}O_4$ are due to the internal surface of the former being more stable than the outer surface, a conjecture that is reinforced by the results of dissolution measurements reported below. We do not, at this stage, have an explanation for the slight dip then rise in capacity within the first few cycles for the mesoporous $Li_{1.12}Mn_{1.88}O_4$; powder-XRD data show no evidence of structural changes on cycling.

To explore whether the superior capacity retention of the mesoporous $Li_{1.12}Mn_{1.88}O_4$ compared with the other materials is associated with less manganese dissolution, equal masses of the mesoporous, bulk, and nanoparticulate $Li_{1.12}Mn_{1.88}O_4$ and the bulk $Li_{1.05}Mn_{1.95}O_4$ were placed into equal volumes of electrolyte at 50 °C for 4 days, and the quantity of manganese in each solution was determined (see Experimental Section). The manganese concentrations in the mesoporous $Li_{1.12}Mn_{1.88}O_4$, bulk $Li_{1.12}Mn_{1.88}O_4$, nanoparticulate $Li_{1.12}Mn_{1.88}O_4$, and bulk $Li_{1.05}Mn_{1.95}O_4$ are 3.7, 6.3, 26, and 9.5 ppm, respectively. These results demonstrate that the mesoporous $Li_{1.12}Mn_{1.88}O_4$ is more stable at elevated temperatures than the other materials. Importantly, they reinforce the conclusions from Figure 2C that the stability of the mesoporous $Li_{1.12}Mn_{1.88}O_4$ is slightly greater than the equivalent bulk phase, despite the former having a much higher surface area. The results of the dissolution experiments support the view expressed above that the internal surface of the mesoporous $Li_{1.12}Mn_{1.88}O_4$ is more stable towards disproportionation/dissolution of the manganese than the external surface, explaining the superior cycling stability at elevated temperatures compared with nanoparticles. It is difficult to study directly the internal surfaces of mesoporous solids. XPS measurements carried out on the bulk and mesoporous $Li_{1.12}Mn_{1.88}O_4$ (see Supporting Information Figure 3S) give an average oxidation state of +3.65 for manganese on the outer surface, that is, the surface is not $Li_2MnO_3$.

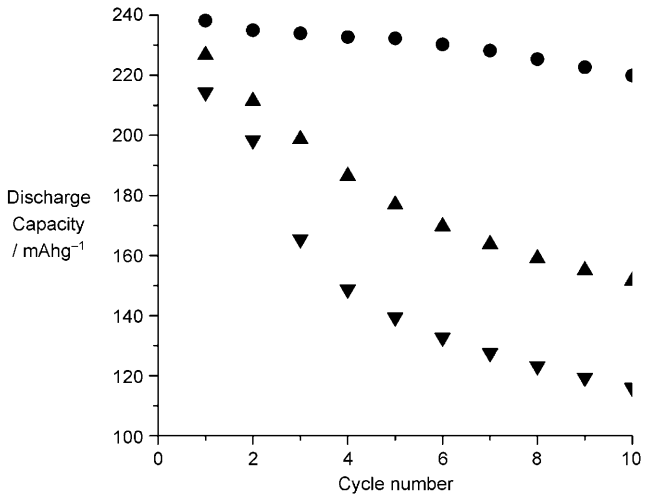


***Figure 3.*** Discharge capacity versus cycle number for the mesoporous $Li_{1.12}Mn_{1.88}O_4$ (●), bulk $Li_{1.05}Mn_{1.95}O_4$ (▲), and bulk $Li_{1.12}Mn_{1.88}O_4$ (▼) at a rate of 30 mA g$^{-1}$ (0.30C) between 2–4.5 V.

Cycling over the 3 and 4 V plateaus were also considered. Although not as technologically relevant as the 4 V region, it is interesting to explore the effect that mesostructuring has on such cycling. The variation of the discharge capacity with the cycle number, where cycling is carried out between 2 and 4.5 V, is shown in Figure 3 for the bulk $Li_{1.05}Mn_{1.95}O_4$, and the mesoporous and bulk $Li_{1.12}Mn_{1.88}O_4$. Even within 10 cycles the severe capacity fading of the bulk materials is evident, whereas the mesoporous $Li_{1.12}Mn_{1.88}O_4$ exhibits much better capacity retention. To consider this effect in more detail the load curves for each of the three materials as a function of cycle number were examined. It is known that the capacity loss suffered on cycling bulk spinel with the composition $Li_{1.05}Mn_{1.95}O_4$ between 3 and 4 V plateaus is related to the difficulty of reversing the cubic ($LiMn_2O_4$)/tetragonal-($Li_2Mn_2O_4$) phase transition associated with the 3 V plateau.[32,33] As a result, although capacity lowering occurs at both 3 and 4 V, the most severe loss of capacity is associated with the 3 V plateau for the bulk $Li_{1.05}Mn_{1.95}O_4$ (Figure 4A). This is also the case for the bulk $Li_{1.12}Mn_{1.88}O_4$ material (Figure 4B), although in this case there is more loss of capacity at 4 V than for the $Li_{1.05}Mn_{1.95}O_4$ electrode. In contrast, the load curves for the mesoporous $Li_{1.12}Mn_{1.88}O_4$ presents a more optimistic situation (Figure 4C). The most

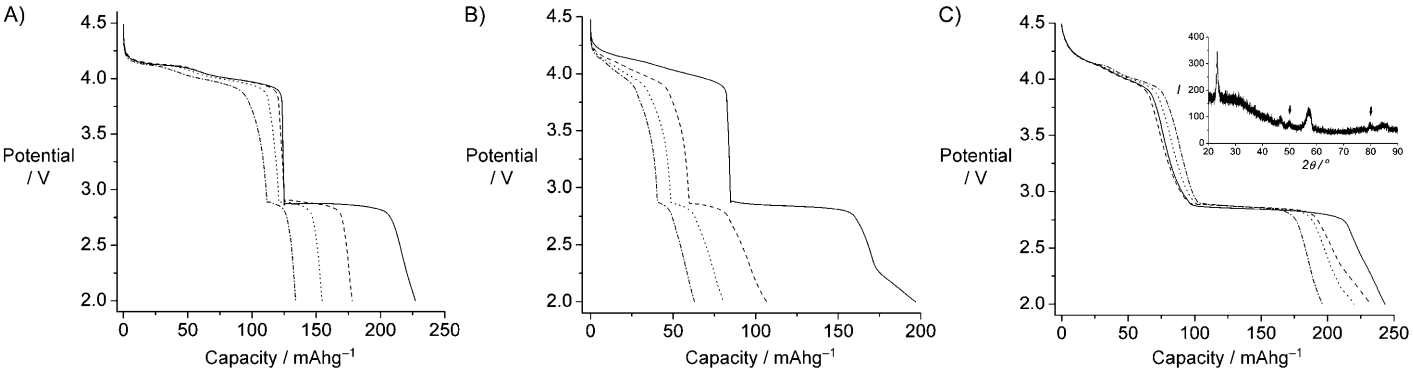


***Figure 4.*** Load curves showing the first discharge (——), fifth discharge (– – –), tenth discharge (•••••) and 20th discharge (–•–•) for A) bulk $Li_{1.05}Mn_{1.95}O_4$, B) bulk $Li_{1.12}Mn_{1.88}O_4$, and C) mesoporous $Li_{1.12}Mn_{1.88}O_4$. The inset in (C) is the powder XRD pattern for mesoporous $Li_{1.12}Mn_{1.88}O_4$ after discharging to 2 V; arrows indicate peaks for the tetragonal phase.

  

dramatic difference occurs at 3 V, where the capacity retention is far better than for either of the bulk materials, implying that the cubic/tetragonal phase transformation is far more facile for the mesoporous material than the bulk. The capacity retention at 4 V is also somewhat better for the mesoporous material. The inset in Figure 4C shows powder XRD data collected at the end of discharge demonstrating the presence of the tetragonal phase at the end of the 3 V plateau.

TEM data collected after cycling over the 3 and 4 V plateaus demonstrate retention of the mesostructure (Figure 1A (f)). As the nanometer-sized walls in the mesoporous materials lead to the relief of strain during the structural phase transitions, these materials undergo the transitions in a more facile fashion than their bulk counterparts.[15] Indeed the transformations from $Mn_2O_3$ to $Mn_3O_4$ and then to $LiMn_2O_4$, associated with the formation of the mesoporous material discussed herein, while retaining the mesostructure throughout, are a testimony to the ease with which the phase transformations can occur in mesoporous materials. It appears that this same effect has rendered more facile the cubic/tetragonal phase transition than is the case for the bulk materials. These results are in agreement with previous studies on spinels. On cycling layered $LiMnO_2$, it coverts to a spinel material that exhibits a nanodomain structure, in which the domains can spontaneously switch between cubic and tetragonal phases, with strain being relieved at the domain wall boundaries.[32,33] Furthermore, ball-milling $LiMn_2O_4$ can induce a similar nanodomain structure with a consequent improvement in cycling over the 3 V plateau.[34]

In conclusion, a mesoporous lithium manganese oxide spinel has been synthesized for the first time. By combining a mesoporous structure with the composition $Li_{1.12}Mn_{1.88}O_4$, superior rate capability at ambient temperature (50% higher specific capacity and marginally higher volumetric capacity at 3000 mA h $g^{-1}$, 30C) compared with the corresponding bulk material have been demonstrated. Comparable stability to the bulk material at elevated temperatures is observed despite a surface area of 90 $m^2 g^{-1}$ for the mesopore and without recourse to the introduction of foreign ion dopants or the application of metal oxide coatings, suggesting that the internal surfaces of the mesopore are more stable than the external surface. In addition, the mesoporous material can be cycled over both the 3 and 4 V plateaus with improved capacity retention compared with bulk materials. This improvement is due to the nanometer-sized walls better accommodating the strain of the cubic/tetragonal phase transformation that occurs at 3 V.

## Experimental Section

Preparations of electrode materials: Preparation of the mesoporous silica (KIT-6) has been described previously.[35] Typical synthesis of mesoporous $Li_{1.12}Mn_{1.88}O_4$: $Mn(NO_3)_2{\cdot}6H_2O$ (98%, Aldrich; 30 g) was dissolved in distilled water (ca. 20 mL) and this saturated $Mn(NO_3)_2$ solution (5 mL) was added slowly with stirring to mesoporous KIT-6 (5 g) dispersed in *n*-hexane (200 mL). The mixture was stirred overnight, filtered, and dried at room temperature, followed by heating at 600 °C for 3 h. The resulting material was treated twice with a hot NaOH solution (2 M) in water to remove the silica template, followed by washing with water and drying at 60 °C. This procedure results in mesoporous $Mn_2O_3$ free from $SiO_2$, as demonstrated by chemical analysis. Reduction of mesoporous $Mn_2O_3$ to $Mn_3O_4$ was achieved by heating at 280 °C for 3 h under a $H_2$ atmosphere ($H_2$/Ar = 5:95). Thereafter, mesoporous $Mn_3O_4$ (1 g) was mixed with $LiOH{\cdot}H_2O$ (1.5 g) in water (10 mL), stirred until dry, and was heated slowly at 350 °C for 1 h. After the calcination, the sample was cooled to room temperature at a rate of 3 °C $min^{-1}$, and the resulting material was washed with water then dried at 120 °C.

Bulk $Li_{1.05}Mn_{1.95}O_4$ and $Li_{1.12}Mn_{1.88}O_4$: stoichiometric ratios of lithium acetate and manganese acetate were ball-milled for 15 min before heating at 400 °C in air for 3 h. The resulting powder was ball-milled again for 15 min and then heated at 900 °C in air for 5 h. After the calcination, the sample was cooled to room temperature at a rate of 3 °C $min^{-1}$.

Nanoparticles of $Li_{1.05}Mn_{1.95}O_4$ and $Li_{1.12}Mn_{1.88}O_4$ were synthesized from lithium acetate and manganese acetate following a previously reported procedure.[36]

The materials were characterized by transmission electron microscopy (TEM, Jeol JEM-2011), powder-XRD diffraction (PXRD, Stoe STADI/P diffractometer operating in transmission mode with $Fe_{K\alpha_1}$ radiation, $\lambda = 1.936$ Å), and $N_2$ sorption (Hiden IGA porosimeter) techniques. Oxidation states were determined by redox titration using ferrous ammonium sulfate/$KMnO_4$, as described previously.[37] Atomic absorption measurements were carried out on a Pye Unicam AAS spectrometer.

Manganese dissolution studies: spinel material (0.1 g) was sealed in a glass bottle with LP-30 electrolyte (10 mL) and stored at 50 °C for 4 days. After filtering, the liquid was collected and analyzed by atomic absorption.

Electrochemical cells were constructed by mixing the active material, Kynar (a copolymer based on poly(vinylidene fluoride)), and Super S carbon in the weight ratios 80:10:10. The mixture was cast onto aluminum foil from acetone using the doctor-blade technique. After solvent evaporation at room temperature and heating at 80 °C under vacuum for 8 h, the electrodes were assembled into cells with a lithium electrode (99.9%, Aldrich; a disc with a diameter of 8 mm and a thickness of ca. 0.7 mm) and LP-30 electrolyte (Merck; 1 M $LiPF_6$ in 1:1 v/v ethylene carbonate/dimethyl carbonate). The cells were constructed and handled in an argon-filled MBraun glovebox. Electrochemical measurements were carried out using a MACCOR Series 4200 cycler. High-rate measurements were performed on two and three electrode cells, but no difference was found, demonstrating that the polarization was dominated by the cathode. Hence two-electrode results are reported here.

Received: July 15, 2008
Published online: November 6, 2008

**Keywords:** electrodes · intercalation · lithium batteries · mesoporous materials · spinel phases

[1] M. M. Thackeray, W. I. F. David, P. G. Bruce, J. B. Goodenough, *Mater. Res. Bull.* **1983**, *18*, 461.
[2] J. M. Tarascon, E. Wang, F. K. Shokoohi, W. R. McKinnon, S. Colson, *J. Electrochem. Soc.* **1991**, *138*, 2859.
[3] W. A. van Schalkwijk, B. Scrosati, *Advances in Lithium-ion Batteries*, Kluwer Academic/Plenum, New York, **2002**.
[4] G. A. Nazri, G. Pistoia, *Lithium Batteries: Science and Technology*, Kluwer Academic, Boston, **2004**.
[5] J. M. Tarascon, M. Armand, *Nature* **2001**, *414*, 359.
[6] A. S. Aricò, P. Bruce, B. Scrosati, J. M. Tarascon, W. Van Schalkwijk, *Nat. Mater.* **2005**, *4*, 366.
[7] P. G. Bruce, B. Scrosati, J. M. Tarascon, *Angew. Chem.* **2008**, *120*, 2972; *Angew. Chem. Int. Ed.* **2008**, *47*, 2930.
[8] R. J. Gummow, A. Dekock, M. M. Thackeray, *Solid State Ionics* **1994**, *69*, 59.

  

[9] Y. Y. Xia, M. Yoshio, *J. Electrochem. Soc.* **1997**, *144*, 4186.
[10] G. Amatucci, J. M. Tarascon, *J. Electrochem. Soc.* **2002**, *149*, K31.
[11] K. Ariyoshi, E. Iwata, M. Kuniyoshi, H. Wakabayashi, T. Ohzuku, *Electrochem. Solid-State Lett.* **2006**, *9*, A557.
[12] Z. H. Chen, K. Amine, *J. Electrochem. Soc.* **2006**, *153*, A1279.
[13] A. Du Pasquier, A. Blyr, P. Courjal, D. Larcher, G. Amatucci, B. Gerand, J. M. Tarascon, *J. Electrochem. Soc.* **1999**, *146*, 428.
[14] Y. Y. Xia, Y. H. Zhou, M. Yoshio, *J. Electrochem. Soc.* **1997**, *144*, 2593.
[15] F. Jiao, J. C. Jumas, M. Womes, A. V. Chadwick, A. Harrison, P. G. Bruce, *J. Am. Chem. Soc.* **2006**, *128*, 12905.
[16] F. Jiao, K. M. Shaju, P. G. Bruce, *Angew. Chem.* **2005**, *117*, 6708; *Angew. Chem. Int. Ed.* **2005**, *44*, 6550.
[17] A. H. Lu, F. Schuth, *Adv. Mater.* **2006**, *18*, 1793.
[18] R. Ryoo, S. H. Joo, M. Kruk, M. Jaroniec, *Adv. Mater.* **2001**, *13*, 677.
[19] H. F. Yang, D. Y. Zhao, *J. Mater. Chem.* **2005**, *15*, 1217.
[20] F. Jiao, P. G. Bruce, *Adv. Mater.* **2007**, *19*, 657.
[21] F. Jiao, A. Harrison, J. C. Jumas, A. V. Chadwick, W. Kockelmann, P. G. Bruce, *J. Am. Chem. Soc.* **2006**, *128*, 5468.
[22] C. Dickinson, W. Z. Zhou, R. P. Hodgkins, Y. F. Shi, D. Y. Zhao, H. Y. He, *Chem. Mater.* **2006**, *18*, 3088.
[23] J. Y. Luo, J. J. Zhang, Y. Y. Xia, *Chem. Mater.* **2006**, *18*, 5618.
[24] A. Rumplecker, F. Kleitz, E. L. Salabas, F. Schuth, *Chem. Mater.* **2007**, *19*, 485.
[25] W. H. Shen, X. P. Dong, Y. F. Zhu, H. R. Chen, J. L. Shi, *Microporous Mesoporous Mater.* **2005**, *85*, 157.
[26] C. Masquelier, M. Tabuchi, K. Ado, R. Kanno, Y. Kobayashi, Y. Maki, O. Nakamura, J. B. Goodenough, *J. Solid State Chem.* **1996**, *123*, 255.
[27] M. M. Thackeray, P. J. Johnson, L. A. Depicciotto, P. G. Bruce, J. B. Goodenough, *Mater. Res. Bull.* **1984**, *19*, 179.
[28] Y. M. Chiang, D. R. Sadoway, Y. I. Jang, B. Y. Huang, H. F. Wang, *Electrochem. Solid-State Lett.* **1999**, *2*, 107.
[29] W. Choi, A. Manthiram, *J. Electrochem. Soc.* **2007**, *154*, A614.
[30] Y. K. Sun, K. J. Hong, J. Prakash, *J. Electrochem. Soc.* **2003**, *150*, A970.
[31] Y. Y. Xia, M. Yoshio, *J. Power Sources* **1997**, *66*, 129.
[32] A. D. Robertson, A. R. Armstrong, P. G. Bruce, *Chem. Mater.* **2001**, *13*, 2380.
[33] H. F. Wang, Y. I. Jang, Y. M. Chiang, *Electrochem. Solid-State Lett.* **1999**, *2*, 490.
[34] S. H. Kang, J. B. Goodenough, L. K. Rabenberg, *Chem. Mater.* **2001**, *13*, 1758.
[35] F. Kleitz, S. H. Choi, R. Ryoo, *Chem. Commun.* **2003**, 2136.
[36] A. Caballero, M. Cruz, L. Hernan, M. Melero, J. Morales, E. R. Castellon, *J. Power Sources* **2005**, *150*, 192.
[37] M. J. Katz, R. C. Clarke, W. F. Nye, *Anal. Chem.* **1956**, *28*, 507.

  